EUROPEAN ORGANIZATION FOR NUCLEAR RESEARCH (CERN)

CERN-EP/2000-093
July 3, 2000

A Measurement of the *b*-quark Mass from Hadronic Z Decays

The ALEPH Collaboration

Abstract

Hadronic Z decay data taken with the ALEPH detector at LEP1 are used to measure the three-jet rate as well as moments of various event-shape variables. The ratios of the observables obtained from b-tagged events and from an inclusive sample are determined. The mass of the b quark is extracted from a fit to the measured ratios using a next-to-leading order prediction including mass effects. Taking the first moment of the y_3 distribution, which is the observable with the smallest hadronization corrections and systematic uncertainties, the result is

$$m_b(M_{\mathrm{Z}}) = [3.27 \pm 0.22(\mathrm{stat}) \pm 0.22(\mathrm{exp}) \pm 0.38(\mathrm{had}) \pm 0.16(\mathrm{theo})] \ \mathrm{GeV}/c^2 \quad .$$

The measured ratio is alternatively employed to test the flavour independence of the strong coupling constant for b and light quarks.

submitted to European Physical Journal C

The ALEPH Collaboration

R. Barate, D. Decamp, P. Ghez, C. Goy, J.-P. Lees, E. Merle, M.-N. Minard, B. Pietrzyk

Laboratoire de Physique des Particules (LAPP), IN^{2}P^3-CNRS, F-74019 Annecy-le-Vieux Cedex, France

S. Bravo, M.P. Casado, M. Chmeissani, J.M. Crespo, E. Fernandez, M. Fernandez-Bosman, Ll. Garrido,[15] E. Graugés, M. Martinez, G. Merino, R. Miquel, Ll.M. Mir, A. Pacheco, H. Ruiz

Institut de Física d'Altes Energies, Universitat Autònoma de Barcelona, E-08193 Bellaterra (Barcelona), Spain[7]

A. Colaleo, D. Creanza, M. de Palma, G. Iaselli, G. Maggi, M. Maggi, S. Nuzzo, A. Ranieri, G. Raso, F. Ruggieri, G. Selvaggi, L. Silvestris, P. Tempesta, A. Tricomi,[3] G. Zito

Dipartimento di Fisica, INFN Sezione di Bari, I-70126 Bari, Italy

X. Huang, J. Lin, Q. Ouyang, T. Wang, Y. Xie, R. Xu, S. Xue, J. Zhang, L. Zhang, W. Zhao

Institute of High Energy Physics, Academia Sinica, Beijing, The People's Republic of China[8]

D. Abbaneo, G. Boix,[6] O. Buchmüller, M. Cattaneo, F. Cerutti, G. Dissertori, H. Drevermann, R.W. Forty, M. Frank, T.C. Greening, A.W. Halley, J.B. Hansen, J. Harvey, P. Janot, B. Jost, I. Lehraus, P. Mato, A. Minten, A. Moutoussi, F. Ranjard, L. Rolandi, D. Schlatter, M. Schmitt,[20] O. Schneider,[2] P. Spagnolo, W. Tejessy, F. Teubert, E. Tournefier, A.E. Wright

European Laboratory for Particle Physics (CERN), CH-1211 Geneva 23, Switzerland

Z. Ajaltouni, F. Badaud, G. Chazelle, O. Deschamps, A. Falvard, P. Gay, C. Guicheney, P. Henrard, J. Jousset, B. Michel, S. Monteil, J-C. Montret, D. Pallin, P. Perret, F. Podlyski

Laboratoire de Physique Corpusculaire, Université Blaise Pascal, IN^{2}P^3-CNRS, Clermont-Ferrand, F-63177 Aubière, France

J.D. Hansen, J.R. Hansen, P.H. Hansen,[1] B.S. Nilsson, A. Wäänänen

Niels Bohr Institute, DK-2100 Copenhagen, Denmark[9]

G. Daskalakis, A. Kyriakis, C. Markou, E. Simopoulou, A. Vayaki

Nuclear Research Center Demokritos (NRCD), GR-15310 Attiki, Greece

A. Blondel,[12] G. Bonneaud, J.-C. Brient, A. Rougé, M. Rumpf, M. Swynghedauw, M. Verderi, H. Videau

Laboratoire de Physique Nucléaire et des Hautes Energies, Ecole Polytechnique, IN^{2}P^3-CNRS, F-91128 Palaiseau Cedex, France

E. Focardi, G. Parrini, K. Zachariadou

Dipartimento di Fisica, Università di Firenze, INFN Sezione di Firenze, I-50125 Firenze, Italy

A. Antonelli, M. Antonelli, G. Bencivenni, G. Bologna,[4] F. Bossi, P. Campana, G. Capon, V. Chiarella, P. Laurelli, G. Mannocchi,[5] F. Murtas, G.P. Murtas, L. Passalacqua, M. Pepe-Altarelli

Laboratori Nazionali dell'INFN (LNF-INFN), I-00044 Frascati, Italy

J.G. Lynch, P. Negus, V. O'Shea, C. Raine, P. Teixeira-Dias, A.S. Thompson

Department of Physics and Astronomy, University of Glasgow, Glasgow G12 8QQ,United Kingdom[10]

R. Cavanaugh, S. Dhamotharan, C. Geweniger,[1] P. Hanke, G. Hansper, V. Hepp, E.E. Kluge, A. Putzer, J. Sommer, K. Tittel, S. Werner,[19] M. Wunsch[19]

Kirchhoff-Institut fr Physik, Universität Heidelberg, D-69120 Heidelberg, Germany[16]

R. Beuselinck, D.M. Binnie, W. Cameron, P.J. Dornan, M. Girone, N. Marinelli, J.K. Sedgbeer, J.C. Thompson,[14] E. Thomson[22]

Department of Physics, Imperial College, London SW7 2BZ, United Kingdom[10]

V.M. Ghete, P. Girtler, E. Kneringer, D. Kuhn, G. Rudolph
Institut für Experimentalphysik, Universität Innsbruck, A-6020 Innsbruck, Austria[18]

C.K. Bowdery, P.G. Buck, A.J. Finch, F. Foster, G. Hughes, R.W.L. Jones, N.A. Robertson
Department of Physics, University of Lancaster, Lancaster LA1 4YB, United Kingdom[10]

I. Giehl, K. Jakobs, K. Kleinknecht, G. Quast,[1] B. Renk, E. Rohne, H.-G. Sander, H. Wachsmuth, C. Zeitnitz
Institut für Physik, Universität Mainz, D-55099 Mainz, Germany[16]

A. Bonissent, J. Carr, P. Coyle, O. Leroy, P. Payre, D. Rousseau, M. Talby
Centre de Physique des Particules, Université de la Méditerranée, IN^{2}P^3-CNRS, F-13288 Marseille, France

M. Aleppo, F. Ragusa
Dipartimento di Fisica, Università di Milano e INFN Sezione di Milano, I-20133 Milano, Italy

H. Dietl, G. Ganis, A. Heister, K. Hüttmann, G. Lütjens, C. Mannert, W. Männer, H.-G. Moser, S. Schael, R. Settles,[1] H. Stenzel, W. Wiedenmann, G. Wolf
Max-Planck-Institut für Physik, Werner-Heisenberg-Institut, D-80805 München, Germany[16]

P. Azzurri, J. Boucrot,[1] O. Callot, S. Chen, A. Cordier, M. Davier, L. Duflot, J.-F. Grivaz, Ph. Heusse, A. Jacholkowska,[1] F. Le Diberder, J. Lefrançois, A.-M. Lutz, M.-H. Schune, J.-J. Veillet, I. Videau,[1] D. Zerwas
Laboratoire de l'Accélérateur Linéaire, Université de Paris-Sud, IN^{2}P^3-CNRS, F-91898 Orsay Cedex, France

G. Bagliesi, T. Boccali, G. Calderini, V. Ciulli, L. Foà, A. Giassi, F. Ligabue, A. Messineo, F. Palla,[1] G. Rizzo, G. Sanguinetti, A. Sciabà, G. Sguazzoni, R. Tenchini,[1] A. Venturi, P.G. Verdini
Dipartimento di Fisica dell'Università, INFN Sezione di Pisa, e Scuola Normale Superiore, I-56010 Pisa, Italy

G.A. Blair, G. Cowan, M.G. Green, T. Medcalf, J.A. Strong, J.H. von Wimmersperg-Toeller
Department of Physics, Royal Holloway & Bedford New College, University of London, Surrey TW20 OEX, United Kingdom[10]

R.W. Clifft, T.R. Edgecock, P.R. Norton, I.R. Tomalin
Particle Physics Dept., Rutherford Appleton Laboratory, Chilton, Didcot, Oxon OX11 OQX, United Kingdom[10]

B. Bloch-Devaux, P. Colas, S. Emery, W. Kozanecki, E. Lançon, M.-C. Lemaire, E. Locci, P. Perez, J. Rander, J.-F. Renardy, A. Roussarie, J.-P. Schuller, J. Schwindling, A. Trabelsi,[21] B. Vallage
CEA, DAPNIA/Service de Physique des Particules, CE-Saclay, F-91191 Gif-sur-Yvette Cedex, France[17]

S.N. Black, J.H. Dann, R.P. Johnson, H.Y. Kim, N. Konstantinidis, A.M. Litke, M.A. McNeil, G. Taylor
Institute for Particle Physics, University of California at Santa Cruz, Santa Cruz, CA 95064, USA[13]

C.N. Booth, S. Cartwright, F. Combley, M. Lehto, L.F. Thompson
Department of Physics, University of Sheffield, Sheffield S3 7RH, United Kingdom[10]

K. Affholderbach, A. Böhrer, S. Brandt, C. Grupen,[1] A. Misiejuk, G. Prange, U. Sieler
Fachbereich Physik, Universität Siegen, D-57068 Siegen, Germany[16]

G. Giannini, B. Gobbo
Dipartimento di Fisica, Università di Trieste e INFN Sezione di Trieste, I-34127 Trieste, Italy

J. Rothberg, S. Wasserbaech
Experimental Elementary Particle Physics, University of Washington, Seattle, WA 98195 U.S.A.

S.R. Armstrong, K. Cranmer, P. Elmer, D.P.S. Ferguson, Y. Gao, S. González, O.J. Hayes, H. Hu, S. Jin, J. Kile,

P.A. McNamara III, J. Nielsen, W. Orejudos, Y.B. Pan, Y. Saadi, I.J. Scott, J. Walsh, Sau Lan Wu, X. Wu, G. Zobernig

Department of Physics, University of Wisconsin, Madison, WI 53706, USA[11]

[1]Also at CERN, 1211 Geneva 23, Switzerland.
[2]Now at Université de Lausanne, 1015 Lausanne, Switzerland.
[3]Also at Dipartimento di Fisica di Catania and INFN Sezione di Catania, 95129 Catania, Italy.
[4]Also Istituto di Fisica Generale, Università di Torino, 10125 Torino, Italy.
[5]Also Istituto di Cosmo-Geofisica del C.N.R., Torino, Italy.
[6]Supported by the Commission of the European Communities, contract ERBFMBICT982894.
[7]Supported by CICYT, Spain.
[8]Supported by the National Science Foundation of China.
[9]Supported by the Danish Natural Science Research Council.
[10]Supported by the UK Particle Physics and Astronomy Research Council.
[11]Supported by the US Department of Energy, grant DE-FG0295-ER40896.
[12]Now at Departement de Physique Corpusculaire, Université de Genève, 1211 Genève 4, Switzerland.
[13]Supported by the US Department of Energy, grant DE-FG03-92ER40689.
[14]Also at Rutherford Appleton Laboratory, Chilton, Didcot, UK.
[15]Permanent address: Universitat de Barcelona, 08208 Barcelona, Spain.
[16]Supported by the Bundesministerium für Bildung, Wissenschaft, Forschung und Technologie, Germany.
[17]Supported by the Direction des Sciences de la Matière, C.E.A.
[18]Supported by the Austrian Ministry for Science and Transport.
[19]Now at SAP AG, 69185 Walldorf, Germany.
[20]Now at Harvard University, Cambridge, MA 02138, U.S.A.
[21]Now at Département de Physique, Faculté des Sciences de Tunis, 1060 Le Belvédère, Tunisia.
[22]Now at Department of Physics, Ohio State University, Columbus, OH 43210-1106, U.S.A.

1 Introduction

The advent of next-to-leading order (NLO) calculations for e^+e^- annihilation into quark pairs, which take full account of quark mass effects [1, 2, 3, 4], has opened up the possibility for further investigations of QCD, such as measurements of the flavour independence of the strong coupling constant [5, 6, 7] or measurements of the running b-quark mass at the Z mass scale [5, 8]. The b-quark mass is one of the fundamental parameters of the Standard Model Lagrangian, and can in principle be viewed as a parameter similar to the coupling constant. The renormalization procedure leads to the definition of a running quantity, the renormalized b-quark mass, which is a function of the renormalization scale. An interpretation as a particle mass is difficult because of the fact that quarks are not asymptotically free states. Nevertheless, a definition of the mass as the pole of the quark propagator is used frequently, which, depending on the size of long-distance QCD effects, can be interpreted as the mass of an (almost) free particle.

Most of the b-quark mass determinations have been performed at rather low scales [9]. It is therefore interesting to measure this parameter at a large scale. Previous measurements have used the ratio of three-jet rates in b- and uds-quark decays of the Z boson. For a running b-quark mass of about $3\,\mathrm{GeV}/c^2$ a 3% deviation from unity is observed in this ratio [5]. This is because the large b-quark mass suppresses gluon radiation in a similar way to the suppression of bremsstrahlung for muons compared to electrons.

In this analysis a set of event-shape observables has been employed in addition to the three-jet rate in order to study the b-quark mass dependence of the measured ratios of the observables in b and uds initiated events. The suppression of gluon radiation by the b-quark mass affects the event-shape distributions, and these variables have rather different behaviour with respect to the hadronization and next-to-leading order effects. The final result is derived using the first moment of the y_3 distribution, which is the least affected by hadronization and next-to-leading order corrections.

In the following section the analysis method is outlined, then a description of the ALEPH detector is given, followed by a summary of the data analysis. In Section 4 the results for the measurements of the ratios of observables in b and uds events are given, which are then used to determine the b-quark mass in Section 5. A test of the flavour independence of the strong coupling constant is described in Section 6, and the conclusions are given in Section 7.

2 The analysis method

The running b-quark mass enters into the theoretical prediction for the ratio

$$R_{bl}^{\mathrm{pert}} = \frac{O_b}{O_l} \quad , \tag{1}$$

where O_b and O_l are infrared and collinear safe observables at the perturbative level (quarks and gluons) for Z decays into b and light ($l = uds$) quark pairs, respectively. The measured ratio R_{bq}^{meas} of the observables in b-tagged events and in an all-flavour inclusive sample can be related to the quantities at the parton level via the following formula:

$$R_{bq}^{\mathrm{meas}} = (O_b\, H_b\, D_b\, T_b\, \mathcal{P}_b \,+\, O_c\, H_c\, D_c\, T_c\, \mathcal{P}_c \,+\, O_l\, H_l\, D_l\, T_l\, \mathcal{P}_l) \;/\; O_q^{\mathrm{meas}} \quad . \tag{2}$$

Here H_x, D_x, T_x are the corrections due to hadronization, detector effects and tagging, respectively, and $\mathcal{P}_x$ are the purities of the tagged sample, where x is the true flavour. The tagging corrections take into account biases introduced by the flavour tag. The denominator O_q^{meas} can be rewritten as

$$O_q^{\text{meas}} = R_b\, O_b\, H_b\, D_b + R_c\, O_c\, H_c\, D_c + (1 - R_b - R_c)\, O_l\, H_l\, D_l \quad , \tag{3}$$

where $R_{b(c)}$ is the ratio of the partial width of the Z to $b(c)$ quarks and the total hadronic width. Taking all these ingredients, the relation between the measured ratio R_{bq}^{meas} and the ratio of interest R_{bl}^{pert} is given by

$$R_{bq}^{\text{meas}} = \frac{R_{bl}^{\text{pert}}\, H_{b/l}\, D_{b/l}\, T_b\, \mathcal{P}_b + R_{cl}^{\text{pert}}\, H_{c/l}\, D_{c/l}\, T_c\, \mathcal{P}_c + T_l\, \mathcal{P}_l}{R_b\, R_{bl}^{\text{pert}}\, H_{b/l}\, D_{b/l} + R_c\, R_{cl}^{\text{pert}}\, H_{c/l}\, D_{c/l} + (1 - R_b - R_c)} \quad , \tag{4}$$

where $H_{b/l} = H_b/H_l$, $D_{b/l} = D_b/D_l$, and the ratio R_{cl}^{pert} is set to 1. A small deviation of this ratio from unity because of the c-quark mass is considered in the systematic studies. All the correction factors and purities are obtained from Monte Carlo (MC) simulations. Because mainly ratios of corrections are involved, some systematic uncertainties cancel.

R_{bl}^{pert} is extracted from the relationship (4) and finally corrected for the contribution of anomalous triangle diagrams [10], in order to relate R_{bl}^{pert} to R_{bd}^{pert} for which the perturbative calculations have been performed. The triangle contributions cancel out in the second ratio. However, they give a contribution of the order of 0.2% to the first.

The following observables O_x have been considered:

- The rate of three-jet events, where the jets are defined by the `DURHAM` clustering algorithm with the `E` recombination scheme [11]. As shown in Ref. [5], the optimal choice of the resolution parameter y_{cut} for the mass determination is 0.02, because it represents a good compromise between the actual size of the mass effect to be measured and the size of backgrounds from other jet topologies.

- The first and second moments of the event-shape variables thrust T, the C parameter, the three-to-two jets transition value y_3 and the total and wide jet broadening, B_T and B_W. The definitions of the observables can be found, e.g., in [12, 13] and references therein. Moments have been chosen instead of distributions because of the better statistical accuracy with which the perturbative predictions can be evaluated by MC integration. Even higher moments would give smaller hadronization uncertainties. However, the NLO corrections typically get larger and the overall mass effects fall below the 3% level.

A list of the leading (LO) and next-to-leading order (NLO) contributions to $1 - R_{bd}^{\text{pert}}$ is given in Table 1 for all variables, both for the running and the pole mass schemes. They have been evaluated for a b-quark mass of 3 GeV/c^2 in the former and 5 GeV/c^2 in the latter case. The computation of these terms is described in detail in Section 5.1. It is found that for some observables such as the jet broadening variables the mass effect is rather large. However, the NLO corrections can also be sizeable, as in the case of the second moment of thrust and the first moment of the wide jet broadening. For such variables it would definitely be necessary to also compute the NNLO contributions in order to obtain a reliable perturbative prediction. Because of

Table 1: Leading (LO) and next-to-leading (NLO) order contributions to $1 - R_{bd}^{\mathrm{pert}}$, for the running mass (run) and the pole mass (pol) schemes. The contributions are evaluated for a running (pole) mass of 3 (5) GeV/c^2. The strong coupling $\alpha_s(M_{\mathrm{Z}})$ is set to 0.119. The values are given for the three-jet rate (DURHAM scheme) and for the event-shape variables thrust T, C parameter, the transition value y_3 for three to two jets (DURHAM scheme), and the total and wide jet broadenings (B_T and B_W). The indices indicate the first or second moment of the event shape variable.

O	LO (run)	NLO (run)	LO (pol)	NLO (pol)
R_3	0.020	0.010	0.056	−0.008
T_1	0.036	0.019	0.076	−0.007
T_2	0.017	0.032	0.043	0.036
C_1	0.044	0.022	0.091	−0.011
C_2	0.021	0.039	0.052	0.043
y_{3_1}	0.032	0.007	0.071	−0.021
y_{3_2}	0.015	0.003	0.032	−0.007
B_{T_1}	0.117	0.006	0.188	−0.074
B_{T_2}	0.036	0.112	0.080	0.123
B_{W_1}	0.117	−0.085	0.188	−0.183
B_{W_2}	0.036	0.016	0.080	−0.013

these observations in the following only those variables are considered for which in both schemes the NLO contribution is clearly smaller than the LO term. This requirement selects the three-jet rate (R_3), the first moments of thrust (T_1), C parameter (C_1), the three-to-two jets transition value (y_{3_1}) and the total jet broadening (B_{T_1}), as well as the second moment of the three-to-two jets transition value (y_{3_2}) and the wide jet broadening (B_{W_2}).

3 The ALEPH detector

The ALEPH detector is described in detail elsewhere [14, 15]. Here only a description of the tracking detectors is given, being the relevant ones for this analysis. Briefly, at the core of the tracking system is a silicon strip vertex detector (VDET). This has two layers, at average radii of 6.5 and 11.3 cm, each providing measurements in both the r-ϕ and r-z views. The spatial resolution for r-ϕ coordinates is 12 μm for normal incidence and varies between 12 and 22 μm for z coordinates, depending on the track polar angle. The angular coverage of the VDET is $|\cos\theta| < 0.85$ for the inner layer and $|\cos\theta| < 0.69$ for the outer layer. The VDET lies within a cylindrical drift chamber (ITC), which measures up to eight coordinates per track in the r-ϕ view, with a resolution of 150 μm. The ITC is in turn enclosed in a large time projection chamber (TPC), lying between radii of 30 and 180 cm. The TPC provides up to 21 three-dimensional coordinates per track, with resolutions in the r-ϕ and r-z views of 180 μm and 500 μm, respectively. The three tracking detectors are surrounded by a superconducting solenoid producing a magnetic field of 1.5 T.

For charged tracks with two VDET coordinates, a transverse momentum resolution of

$\Delta p_T/p_T = 6\times10^{-4} p_T \oplus 0.005$ (p_T in GeV/c) is achieved. The three-dimensional impact parameter resolution is $(25 + 95/p)\,\mu$m (p in GeV/c).

Recently the LEP1 data set has been reprocessed using improved reconstruction algorithms. In particular, a new VDET pattern recognition algorithm allows groups of several nearby tracks, which may share common hits, to be analyzed, in order to find the hit-to-track assignment which minimizes the track fitting χ^2 for the event as a whole. The improvement on the hit association efficiency is more than 2%. Information from the TPC wires, in addition to that obtained from the pads, is used to improve the coordinate resolution by a factor of two in z, and by 30% in r-ϕ for low momentum tracks.

The tracking system is surrounded by electromagnetic and hadronic calorimeters, and together they are used to measure the neutral and charged energy flow.

4 Data analysis

4.1 Event selection

In this analysis data taken at the peak of the Z resonance from 1991 to 1995 are used. A standard hadronic event selection [12] is applied, which is based on charged particles. A cut $|\cos\theta_T| < 0.7$ is imposed, where θ_T is the polar angle of the thrust axis, computed from all charged and neutral particles as obtained from the energy-flow algorithm [16]. This requirement ensures that the events are well contained within the VDET acceptance. According to the MC simulation the event selection is 61.7% efficient. Non-hadronic background, which is dominated by $\tau^+\tau^-$ events, amounts to 0.3% of this sample. After the selection, a sample of 2.3 million hadronic events remains for further analysis.

The analysis also uses 8.8 million simulated hadronic events produced with a generator based on the `JETSET 7.4` parton shower model [17]. The production rates, decay modes and lifetimes of heavy hadrons are adjusted to agree with recent measurements, while heavy quarks are fragmented using the Peterson et al. model [18]. Detector effects are simulated using the `GEANT` package [19]. The MC events are reweighted in order to reproduce the measured values for the gluon splitting rates into $c\bar{c}$ and $b\bar{b}$ pairs, which are $g_{c\bar{c}} = 0.0319 \pm 0.0046$ and $g_{b\bar{b}} = 0.00251 \pm 0.00063$ [20].

The observables described in Section 2 are computed using only charged tracks. This choice is preferred over taking both charged and neutral energy-flow objects, as for this analysis it allows the reduction of the detector related systematic uncertainties to below the 1% level, without reducing the statistics.

For the computation of the three-jet rate, an additional cut on the minimum energy of a jet of 5 GeV is applied, which removes about 5% of all three-jet events. The three-jet rates are 17.7% (18.2%) in data (MC) for b-tagged events, and 19.3% (20.4%) in the inclusive sample. The excess of three-jet events in the MC simulation had been observed previously [12].

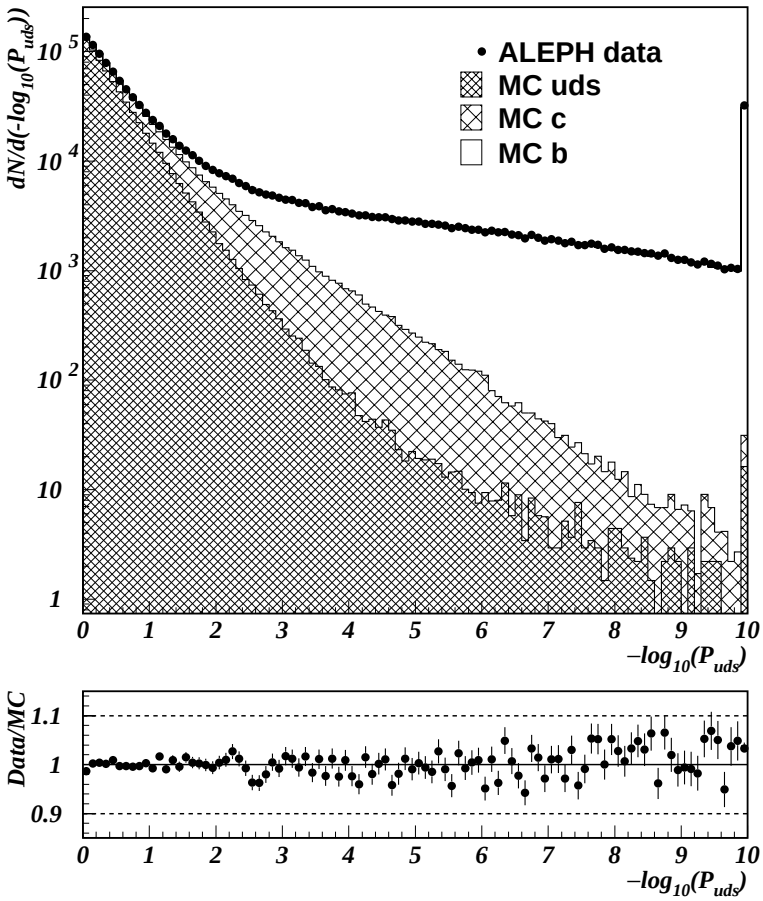

Figure 1: Distribution of the b-tag variable for data and Monte Carlo b, c and uds events. The Monte Carlo has been normalized to the same number of events as the data. The last bin includes overflow entries. The insert at the bottom shows the ratio of data over Monte Carlo.

4.2 The *b*-tag algorithm

The b-tag algorithm, i.e., the criteria used to select b events, follows rather closely the approach described in detail in Ref. [21]. Briefly, the presence of b hadrons is detected using a tag based on the long b hadron lifetime and the precision of the VDET. In contrast to [21], where the tag is applied separately to both hemispheres of the event, here the algorithm uses all tracks of the event.

The actual selection of b events is obtained from a cut on the distribution of the confidence level P_{uds} that all tracks of the event come from the main vertex. This distribution as measured in data and in MC is shown in Fig. 1, together with the expected contributions from different flavours. Very good agreement between data and MC is observed. The requirement $-\log_{10} P_{uds} > 2.2$ selects b events with an efficiency of $\epsilon_b = 80.5\%$ and a purity of $\mathcal{P}_b = 83.1\%$. The backgrounds amount to $\mathcal{P}_c = 13.5\%$ and $\mathcal{P}_l = 3.4\%$.

With this selection, about 488 000 b-tagged events are found in the data before the three-jet

requirement. Out of about 435 000 three-jet events, 86 000 are tagged as $b\bar{b}$.

4.3 Detector and tagging corrections

The observables must be corrected for detector effects, such as acceptance and resolution. This is achieved by computing the observables before and after detector simulation, imposing the same track and event selection cuts as for the data, except for the flavour tag. The ratios of the observables are computed for each true flavour, i.e., the quark flavour of the primary decay products of the Z boson. When computing the observables at the true hadron level before detector simulation, initial state radiation is turned off. In the case of the three-jet rate the detector corrections are $D_b = 0.909$ and $D_l = 0.843$, with a statistical uncertainty at the few per mille level.

The flavour tag can introduce a bias on the measured observables. The bias is estimated by computing the observable before and after applying the tag to the MC sample which passed the event selection cuts, for every flavour. As an example, $T_b = 0.894$ is found for the three-jet rate. Taking the product of ratios of detector corrections, tagging biases and purities the overall detector corrections amount to $D_{b/l}\,T_b\,\mathcal{P}_b = 0.801$, $D_{c/l}\,T_c\,\mathcal{P}_c = 0.112$ and $T_l\,\mathcal{P}_l = 0.045$, again within a statistical accuracy of a few per mille.

4.4 Hadronization corrections

The perturbative predictions are corrected for hadronization effects by computing the relevant observables at parton and at hadron level, including final state photon radiation off quarks. Several Monte Carlo models based on the parton shower approach plus subsequent string or cluster fragmentation are employed for this purpose. For the nominal analysis, the same generator as for the full simulation is used, which is `HVFL` [22]. As already mentioned in Section 4.1, this generator is based on the `JETSET 7.4` parton shower model plus string fragmentation, and in addition the decay modes and lifetimes of heavy hadrons are adjusted to agree with recent measurements. Heavy quarks are fragmented using the Peterson et al. model. The fragmentation parameters for this generator are determined from a global fit to hadronic Z decay data as described in [12], using the present knowledge of heavy quark physics. The modelling of heavy quark physics represents an important part of the systematic uncertainty of the result.

In the `JETSET` parton shower model mass effects are introduced by kinematic constraints to the phase space at each parton branching in the shower evolution as well as by the matching to the leading order matrix element at the first parton branching. The value of M_b (pole mass) is set to $4.75\,\mathrm{GeV}/c^2$. Thirty million events without detector simulation were generated and analyzed. Such a large sample is necessary in order to reduce the statistical error of the hadronization corrections below the one per mille level. These corrections were computed for each flavour individually.

The ratios of hadronization corrections, $H_{b/l}$, are listed in Table 2. The corrections are rather sizeable for almost all the observables; in most cases they are of the same size as or larger than the expected mass effect. Only the three-jet rate and the first two moments of the y_3 distribution have corrections at the 2% level or below. For all the other event-shape variables the corrections are of the order of 10% or even larger. It has been found that the deviation from unity is almost

Table 2: Results for $R_{bd}^{\rm pert}$ with statistical errors, including the uncertainty from the MC statistics. The results are obtained with the hadronization corrections $H_{b/l}$ as predicted by HVFL. Also given are the corrections $H_{b/l}^{nod}$, computed from hadrons directly originating from the string, before any decays (nod=no decays).

O	$R_{bd}^{\rm pert}$	$H_{b/l}$	$H_{b/l}^{nod}$
R_3	0.974 ± 0.005	0.980	0.987
T_1	0.910 ± 0.002	1.134	1.003
C_1	0.894 ± 0.002	1.169	1.009
y_{3_1}	0.955 ± 0.005	1.023	0.987
y_{3_2}	0.979 ± 0.010	0.984	0.984
B_{T_1}	0.831 ± 0.001	1.306	1.025
B_{W_2}	0.929 ± 0.003	1.088	0.986

entirely due to B hadron decays, which change the distributions mainly in the two-jet region. As can be observed from Table 2, the same corrections, computed taking only hadrons which stem directly from the string before any decay, come close to unity within one or two percent. This is in agreement with expectations from recent calculations of nonperturbative power-law corrections to moments of event-shape distributions for massive quarks [23]. The strong dependence on the decays of heavy quarks is taken into account when estimating systematic uncertainties in the following.

4.5 Measurement of $R_{bd}^{\rm pert}$

The correction procedure defined in Eqn. 4 has been carried out individually for every data taking year. The hadronization corrections are taken from the HVFL generator and do not depend on the year. Good agreement between the values of the corrected observable $R_{bl}^{\rm pert}$ in the different years is found, and therefore the final value is obtained from the average over years, weighted according to the statistical errors. The χ^2 confidence level for the combination is 50%. In order to obtain the final values for $R_{bd}^{\rm pert}$, the contributions from anomalous triangle diagrams are first subtracted from the measured ratio $R_{bl}^{\rm pert}$, and then the error due to the finite MC statistics for the evaluation of purities and detector and tagging corrections is added to the statistical error of the data. This statistical error from MC is obtained by evaluating the scatter of results when repeating the analysis with a large number of MC subsamples of smaller size, and then extrapolating the standard deviation thus found to the actual size of the original MC sample. The results are listed in Table 2.

The dependence on the resolution parameter $y_{\rm cut}$ of the perturbative ratio $R_{bd}^{\rm pert}$ for the three-jet rate is indicated in Fig. 2. The data are compared to the predictions of the parton shower models of PYTHIA 6.1, which is based on JETSET, and HERWIG 6.1 [24]. The MC models are in reasonable agreement with the measurement at large $y_{\rm cut}$ values, where the statistical uncertainty is large, however. At intermediate resolution parameters these models predict a lower ratio than observed. In the lowest $y_{\rm cut}$ region, where the resolution parameter approaches the scale of the b-

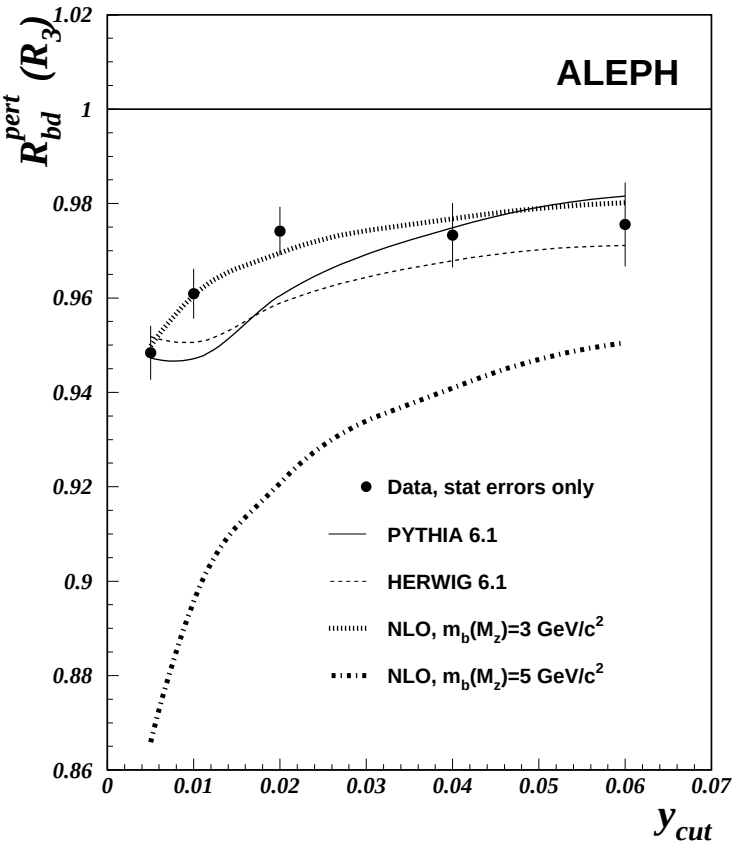

Figure 2: Comparison of the $y_{\rm cut}$ dependence of the measured ratio $R_{bd}^{\rm pert}$ for the three-jet rate to the predictions of parton shower models as well as next-to-leading order (NLO) perturbative QCD for two different values of the b-quark mass in the $\overline{\rm MS}$ scheme. The measurement is obtained using `HVFL` for the hadronization corrections. The errors are statistical only.

mass, a turn-over is observed, which might be interpreted as a short-coming of the approximation for mass effects as implemented in these models.

In addition, in Fig. 2 the next-to-leading order perturbative QCD predictions for two different values of the running b-quark mass in the $\overline{\rm MS}$ scheme are given. The data clearly favour a mass close to 3 GeV/c^2.

4.6 Systematic uncertainties

4.6.1 Detector and physics modelling

Systematic uncertainties can arise from imperfections of the implementation of the physics processes as well as the description of the detector performance. An important physics parameter for the correct description of three-jet rates as well as tagging purities is the gluon splitting rate into heavy quark pairs ($b\bar{b}$, $c\bar{c}$). The MC was reweighted in order to reproduce the most recent

measured values and the experimental uncertainties were propagated to a systematic error on R_{bd}^{pert}.

The MC predictions for the background efficiencies depend on the mean number of VDET coordinates per track and on the assumed impact parameter resolution. It is observed that in the MC simulation more tracks are accepted for use by the b-tag algorithm than in the data, and that the resolution function in impact parameter significance is not perfectly modelled. In order to improve the agreement between data and MC, tracks in the MC are deleted randomly, and a smearing algorithm is applied to the impact parameter significance of some of the MC tracks. A detailed description of this procedure is given in Ref. [21]. The systematic uncertainty related to this procedure is estimated by repeating the whole analysis once without the track deletion, and once without any smearing. Half of the observed deviations in the final result are taken as uncorrelated errors and added in quadrature.

In the case of the three-jet rate additional cuts on the jet quality were studied. Removing the cut on the minimum jet energy results in a relative shift of -0.3% for R_{bd}^{pert}. As a further check of the quality of the MC description of jet quantities, the requirement of at least three charged tracks per jet is applied. This causes a relative change in the result of -0.3%. A relative systematic uncertainty of 0.3% related to the modelling of three-jet events is therefore assumed.

The relative uncertainties due to the physics and detector modelling as described above are listed in Table 3. Adding all these uncertainties in quadrature results in a final experimental systematic error (exp) as quoted in Table 4 for all the observables under consideration.

4.6.2 Hadronization

The uncertainties from the modelling of the hadronization are typically evaluated by computing the hadronization corrections with different MC generators. However, if these uncertainties are to be meaningful, it must be verified that the various models give a good overall description of hadronic Z decay data, and in particular of quantities relevant to the analysis.

As has been shown in Section 4.4, the B hadron decays have a large impact on the size of the hadronization corrections. Because in the tuning of the MC hadronic final states are analyzed after all decays, differences in the description of hadron decays can lead to differences in the tuned fragmentation parameters. In fact, comparing the predictions of the standard `PYTHIA 6.1` and the `HVFL` generator, both based on the `JETSET` parton shower and string fragmentation and tuned to ALEPH data, differences in the fragmentation parameters are found, which translate to a variation in the hadronization corrections, even before considering decays. In order to assess an uncertainty related to the string fragmentation parameters and subsequent decays, the variation in the final result when using `HVFL` or `PYTHIA` for the hadronization corrections is taken as a systematic uncertainty.

Another quantity relevant for this analysis is the b fragmentation function, which describes the energy fraction transferred to the B hadrons during the fragmentation process. In particular, the lower energy tail of the fragmentation function is important for three-jet events. Recently, new measurements of the b fragmentation function have been performed [25, 26]. Both `HVFL` and `PYTHIA` use the Peterson model in their standard setup. In order to test the sensitivity to the b fragmentation function, the measured distribution [25] was included in a global tuning of

the PYTHIA fragmentation parameters, and a new set of hadronization corrections was computed with those parameters. In Ref. [26] it is shown that the Lund fragmentation scheme combined with a model by Bowler [17, 27] gives a good description of the b fragmentation function. The PYTHIA MC was therefore tuned to the data again, but now using the Bowler fragmentation scheme instead of the Peterson model, and new hadronization corrections were derived accordingly. The results obtained with the retuned parameter set and the Bowler fragmentation function were then compared to the standard PYTHIA predictions. The maximum deviation is taken as an estimator of the uncertainty related to the b fragmentation function.

The HERWIG 6.1 MC generator was used for the study of a fragmentation model different from the string approach. As discussed above, differences in the description of hadron decays can effectively lead to differences in the pure fragmentation parameters, after tuning. In order to reduce the sensitivity to this effect, and to study purely the difference between string and cluster fragmentation, the variation in the hadronization corrections for light quarks (uds) only has been propagated into an uncertainty on the final result.

The three components of uncertainty from the hadronization process as described above are listed in Table 3. They are then added in quadrature and quoted as the hadronization uncertainty (had) in Table 4. It is the dominant uncertainty for all variables.

4.6.3 Additional systematic checks

A number of additional systematic checks have been performed in order to evaluate the stability of the results. They are listed in Table 3.

In Eqn. 4 the world average values for R_b and R_c enter. Changing them within their errors has a negligible impact on the results.

An additional factor which contributes to Eqn. 4 is R_{cl}^{pert}, which is the ratio of the observable at parton level for c and light quark events. Because of the smaller c-quark mass this ratio is set to unity in the default analysis. Considering a c-quark mass of $m_c = 1.4\,\mathrm{GeV}/c^2$ leads to very small variations. Only in the case of the total jet broadening is the observed shift larger than the statistical uncertainty; in that case the shift is therefore added in quadrature to the experimental uncertainty.

A possible bias from the b-quark mass in the parton level simulation is estimated by switching off the correction to the massive matrix element for the first branching of a massive quark in the parton shower. For most of the variables, and in particular for the three-jet rate, this results in small variations. As a further cross check, a variant of the JETSET fragmentation model was studied in which the parton shower cutoff parameter Q_0 is increased to 4 GeV. This setting leads to a parton multiplicity of 4 on average, which is close to the multiplicity used in the analytical next-to-leading order calculations. However, it represents a drastic change in the model, and such large cutoff values do not agree with the basic ideas of the parton shower approach. Nevertheless, recomputing R_{bd}^{pert} with the hadronization corrections obtained from this model leads to variations that are well within the fragmentation uncertainty quoted above.

In order to check the stability of the result with respect to the chosen b-tag working point, the cut on the output of the b-tag algorithm was varied over a wide range, which resulted in changes of the purity $\mathcal{P}_b$ from 64% to 95%. For most of the variables, in particular the three-jet

Table 3: Variations (in percent) of R_{bd}^{pert} with respect to the nominal value for all systematic studies performed (PY=PYTHIA). The first block indicates the components of the statistical uncertainty from data and MC, in the second block the experimental uncertainties due to the physics and detector modelling are given, the third block lists the contributions to the systematic uncertainty due to the modelling of hadronization, and the last block gives the results of further systematic checks.

	R_3	T_1	C_1	y_{3_1}	y_{3_2}	B_{T_1}	B_{W_2}
	statistical uncertainties						
Stat. error Data	0.44	0.19	0.15	0.43	0.90	0.11	0.28
Stat. error MC	0.28	0.14	0.11	0.28	0.55	0.07	0.20
	experimental uncertainties						
No hit smearing	−0.47	−0.26	−0.22	−0.42	−0.50	−0.14	−0.36
No track deletion	0.71	0.38	0.29	0.78	1.10	0.17	0.57
$E_{\text{ch}}/\text{Jet} \geq 0$	−0.29	0.00	0.00	0.00	0.00	0.00	0.00
$N_{\text{ch}}/\text{Jet} \geq 3$	−0.28	0.00	0.00	0.00	0.00	0.00	0.00
Gluon splitting	−0.14	0.10	0.16	−0.18	−0.44	0.25	−0.03
	hadronization uncertainties						
Fragm. parameters and B decays	−1.00	0.93	1.42	−0.58	−0.65	3.20	−0.16
Fragm. model	0.64	−3.82	−4.33	0.67	1.56	4.42	−0.89
b fragm. function	0.27	−0.33	−0.41	0.14	0.42	−0.56	−0.22
	additional systematic checks						
c-quark mass effect	−0.03	−0.12	−0.15	−0.09	−0.02	−0.34	−0.11
PY 6.1, $\mathcal{O}(\alpha_s)$ massless	0.40	−2.03	−2.32	0.14	0.60	−2.90	−0.21
PY 6.1, $Q_0 = 4$ GeV	−0.86	1.10	1.47	−0.82	−0.66	3.69	0.27
$-\log_{10} P_{uds} > 1.2$	−0.25	−0.57	−0.71	−0.05	0.13	−0.82	−0.45
$-\log_{10} P_{uds} > 4.0$	0.27	0.82	0.77	0.69	0.67	0.67	0.56
R_{bl}^{meas}	0.03	−0.04	−0.11	0.14	0.30	−0.14	−0.09

rate, the observed deviations in the final result are within the tracking uncertainty as described above. However, in those cases where the deviation exceeds this uncertainty, half of the maximum deviation under variation of the b-tag working point is taken as a systematic uncertainty due to the tracking.

An attempt was made to verify with data the purity $\mathcal{P}_b$ determined from MC. The approach is based on the double tag method as described in [21]. It is possible to extract the hemisphere tagging efficiencies, which then can be related to a global event tagging efficiency if the hemisphere correlations are known. The same working point as in the nominal analysis was chosen. In a first check, R_b and the hemisphere b-tag efficiency ϵ_b^h are measured from the data, whereas all the background efficiencies and the hemisphere correlations are taken from MC. The results are $R_b = 0.2190 \pm 0.0013(\text{stat})$, which is consistent with the world average value, and $\epsilon_b^h = 0.5380 \pm 0.0024(\text{stat})$. Next R_b is fixed to the world average value, and ϵ_b^h as well as the hemisphere

Table 4: Results for $R_{bd}^{\rm pert}$ with statistical (stat), experimental (exp) and hadronization (had) uncertainties.

O	$R_{bd}^{\rm pert}$	$\pm$(stat)	$\pm$(exp)	$\pm$(had)
R_3	0.974	0.005	0.005	0.012
T_1	0.910	0.002	0.004	0.036
C_1	0.894	0.002	0.004	0.041
y_{3_1}	0.955	0.005	0.005	0.009
y_{3_2}	0.979	0.010	0.007	0.017
B_{T_1}	0.831	0.001	0.005	0.046
B_{W_2}	0.929	0.003	0.003	0.009

correlation ρ_b are measured. The result can be translated to the global efficiency by the relation $\epsilon_b = 2\,\epsilon_b^h - (\epsilon_b^h)^2\,(1+\rho_b)$, and then the purity is obtained as

$$\mathcal{P}_b = \frac{R_b\,\epsilon_b}{R_b\,\epsilon_b \;+\; R_c\,\epsilon_c \;+\; (1-R_b-R_c)\,\epsilon_{uds}} \quad . \tag{5}$$

The result is $\mathcal{P}_b = 0.8310 \pm 0.0007$(stat), which is in very good agreement with the value extracted from the MC, $\mathcal{P}_b^{\rm MC} = 0.8305$.

In order to test the overall correction method, an independent set of MC events was analyzed in the same way as the data. Within statistical errors, the extracted $R_{bl}^{\rm pert}$ values are in agreement with the "true" values as found at the parton level of the MC prediction.

Finally, the whole measurement is repeated using the method of Ref. [5], where $R_{bl}^{\rm meas}$ is measured instead of $R_{bq}^{\rm meas}$. Both methods have the same statistical accuracy, but the latter is more simple from the point of view of systematic uncertainties. For the purpose of measuring $R_{bl}^{\rm meas}$ a *uds* tag must also be applied. This is achieved by the requirement $-\log_{10} P_{uds} < 0.5$, which selects light quark events with an efficiency of 66% and a purity of $\mathcal{P}_l = 88\%$. The correction procedure and the correction factors needed are different; nevertheless the results obtained differ from the nominal ones by at most 0.3%.

4.7 Results for $R_{bd}^{\rm pert}$

As stated in Section 4.4, the nominal results are obtained when using `HVFL` for the hadronization corrections. The results for all observables can be found in Table 4, together with statistical and systematic uncertainties. The result for the three-jet rate is in agreement with that of Ref. [5]. Most of the event-shape variables have a better statistical accuracy than the three-jet rate. However, the hadronization uncertainties are rather large.

For the extraction of the *b*-quark mass it is required that the uncertainty on the measured ratio be at the 1% level, and that at the same time the size of the hadronization correction (Table 2) be smaller than the actually measured mass effect, given by the deviation of $R_{bd}^{\rm pert}$ from unity. These requirements leave only the first moment of the y_3 distribution and the three-jet rate for further investigation.

5 Determination of the *b*-quark mass

5.1 Theoretical predictions

The NLO prediction for $R_{bd}^{\rm pert}$ as a function of the observable O and the b-quark mass can be cast in the following form:

$$R_{bd}^{\rm pert}(O) = 1 + r_b(\mu)\left[b_0(r_b(\mu),O) + \frac{\alpha_s(\mu)}{2\pi}b_1(r_b(\mu),O)\right] \;=\; 1 + K(r_b(\mu)) \quad , \tag{6}$$

where $r_b(\mu) = m_b^2(\mu)/M_{\rm Z}^2$, and $m_b(\mu)$ is the running b-quark mass as defined in the $\overline{\rm MS}$ renormalization scheme at the renormalization scale μ. The ratio can also be expressed in terms of the pole mass M_b,

$$R_{bd}^{\rm pert}(O) = 1 + r_b^P\left[b_0^P(r_b^P,O) + \frac{\alpha_s(\mu)}{2\pi}b_1^P(r_b^P,O)\right] \quad , \tag{7}$$

with $r_b^P = M_b^2/M_{\rm Z}^2$. The two predictions are equivalent at this order. The coefficient functions $b_{0,1}$ for the two schemes can be related to each other by expressing the pole mass in terms of the running mass, i.e.,

$$r_b^P = r_b(\mu)\left[1 + \frac{\alpha_s(\mu)}{2\pi}\left(\frac{16}{3} - 4\ln r_b(\mu) + 4\ln\frac{\mu^2}{M_{\rm Z}^2}\right)\right] \quad . \tag{8}$$

The coefficient functions for the three-jet rate were computed in Ref. [1]. For all the other variables they were obtained using the MC generators ZBB4 [4, 28] and EVENT [29]. ZBB4 allows for the integration of the fully differential NLO matrix elements including mass effects, whereas EVENT contains the massless expressions [30]. The latter has been extensively employed at LEP for the calculations of the NLO predictions of event shapes used for the measurements of the strong coupling constant. The differential cross sections for any infrared and collinear safe observable O for either b or d primary quarks in $\rm e^+e^-$ annihilation can be written as

$$\frac{1}{\sigma_{b,d}^{tot}}\frac{d\sigma_{b,d}}{dO} = \frac{\alpha_s}{2\pi}A_{b,d}(O) + \left(\frac{\alpha_s}{2\pi}\right)^2 B_{b,d}(O) \quad . \tag{9}$$

Here $\sigma_{b,d}^{tot}$ is the total cross section for either b or d quark production. The functions A_b, B_b are computed with ZBB4 for fixed values of the b-quark mass in the pole mass scheme, whereas A_d and B_d are obtained from EVENT. Taking the ratio of the cross sections for b and d quarks and expanding up to NLO, the following relationships can be found:

$$r_b^P b_0^P = \frac{A_b}{A_d} - 1 \quad , \tag{10}$$

$$r_b^P b_1^P = \frac{B_b A_d - B_d A_b}{A_d^2} \quad . \tag{11}$$

In order to get the functional dependence of $b_{0,1}^P$ on the b-quark mass, the coefficients A_b and B_b were first computed in very high statistics runs for values of $M_b = 1, 2, 3, 4, 5, 6\,{\rm GeV}/c^2$.

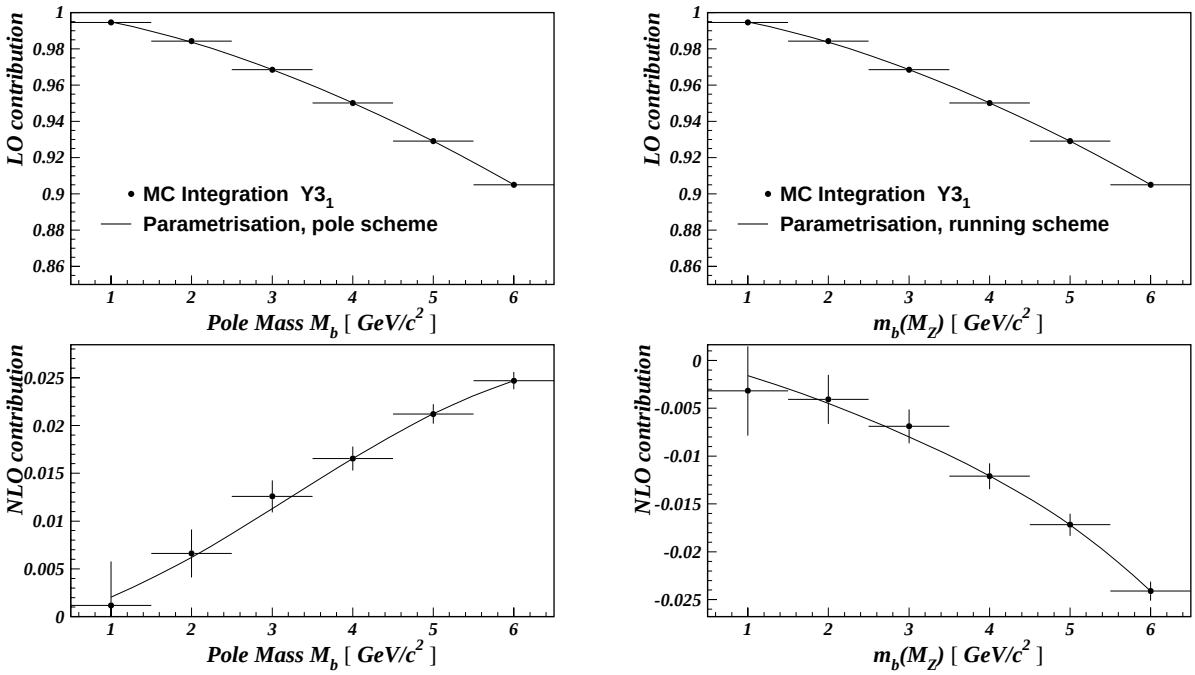

Figure 3: Parametrisations of the b-quark mass dependence for the LO (top) and NLO (bottom) contributions to $R_{bd}^{\rm pert}$ in the pole mass (left) and running mass schemes (right) for the first moment of the y_3 distribution. The points indicate the result of the MC integration, and the full line the parametrisations. The NLO contributions are evaluated using $\alpha_s(M_{\rm Z}) = 0.119$.

The expressions (10) and (11) were then fitted over the relevant range of 3 to 6 GeV/c^2 using parametrisations of the type $c_1 + c_2 r_b^P + c_3 \ln r_b^P$. This functional form follows closely that used in [1]. It has been checked that different parametrisations lead to very small changes in the extracted mass values.

In Fig. 3 an example of these fits is shown for the first moment of the y_3 distribution. With these parametrisations it is possible to estimate the actual quark mass effects in leading order and its next-to-leading order corrections. In Table 1 a list of these LO and NLO contributions is given for all variables for both the running and the pole mass schemes.

Possible evaluations of uncertainties in the mass extraction because of the limited accuracy of the NLO predictions are discussed next. Missing higher order corrections are estimated by extracting firstly the pole mass from the perturbative expression in the pole mass scheme, then translating that result into a running quark mass $m_b(m_b)$ at the b-mass scale, and finally running this mass up to the $M_{\rm Z}$ scale, using the relation

$$r_b(\mu) = r_b(M_{\rm Z}) \left(\frac{\alpha_s(M_{\rm Z})}{\alpha_s(\mu)} \right)^{-4\gamma_0/\beta_0} \quad , \tag{12}$$

where $\alpha_s(\mu) = \alpha_s(M_{\rm Z})/[1 + \alpha_s(M_{\rm Z})\beta_0 \ln(\mu^2/M_{\rm Z}^2)/(4\pi)]$, $\beta_0 = 11 - 2n_f/3$, $n_f = 5$ and $\gamma_0 = 2$. The world average value $\alpha_s(M_{\rm Z}) = 0.119 \pm 0.003$ [31] is used for the strong coupling constant. At NLO the two methods of mass extraction are equivalent. However, the sensitivity to higher

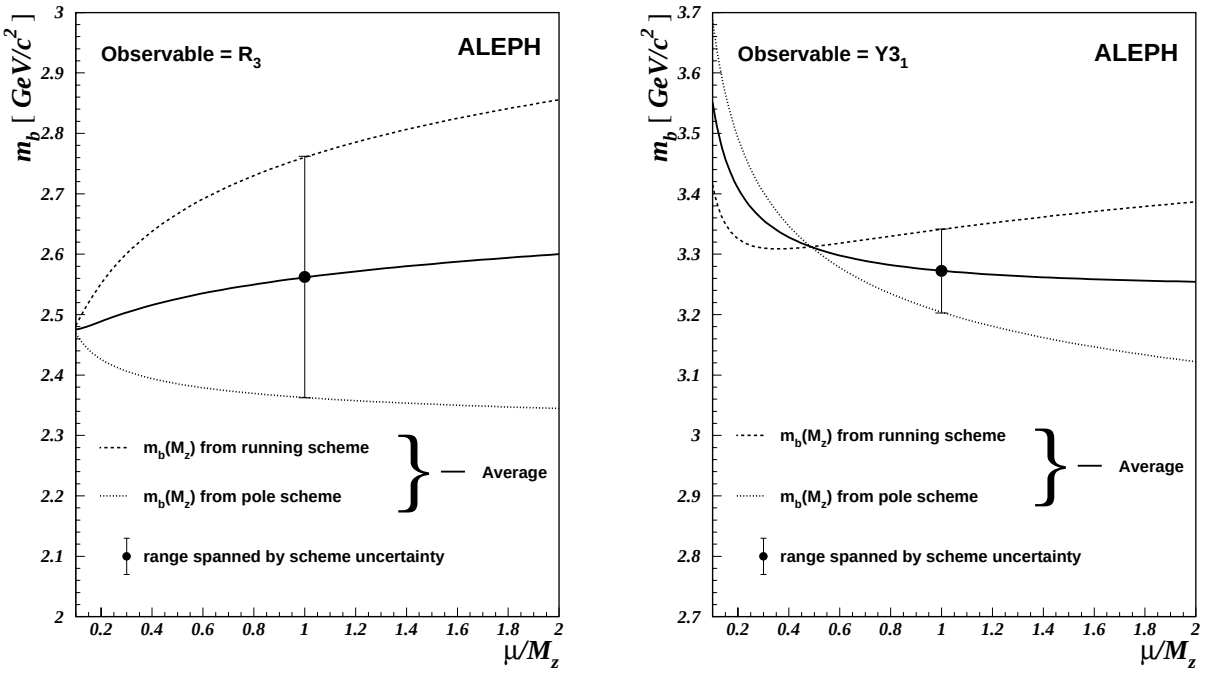

Figure 4: Renormalization scale dependence for the extracted b-quark mass in the running and pole mass scheme, for the observables R_3 (left) and y_{3_1} (right). The error bar spans the range of the scheme uncertainty. The full line indicates the renormalization scale dependence of the average computed from the running and pole mass schemes.

order contributions is different for the two schemes, which can then lead to different results. The shift in the mass when using the pole mass scheme is $-0.14\,\mathrm{GeV}/c^2$ and $-0.4\,\mathrm{GeV}/c^2$ for the y_3 distribution and the three-jet rate, respectively.

In addition, the effects of uncalculated higher order terms can be estimated by a change in the renormalization scale. For the central value $\mu = M_\mathrm{Z}$ is employed, and the systematic error is taken to be half of the range of mass values (average of running and pole mass schemes) found when varying μ from $0.1M_\mathrm{Z}$ to $2M_\mathrm{Z}$. This results in a scale error of $0.15\,\mathrm{GeV}/c^2$ and $0.06\,\mathrm{GeV}/c^2$ for the y_3 distribution and the three-jet rate, respectively. The behaviour of the extracted mass in the two schemes as a function of the renormalization scale μ is illustrated in Fig. 4.

The uncertainty on the world average value for the strong coupling constant has a negligible impact, about $0.01\,\mathrm{GeV}/c^2$, on the measured b-quark mass.

5.2 Results for $m_b(M_\mathrm{Z})$

Based on the predictions obtained above, the running b-quark mass is determined from the measured ratio R_{bd}^{pert} for two observables, the first moment of the y_3 distribution and the three-jet rate. The results are listed in Table 5 together with the statistical and systematic uncertainties, which have been propagated from the corresponding uncertainties on R_{bd}^{pert}. The statistical correlation between the two measurements is 0.66, while the hadronization uncertainties are almost

Table 5: Measured b-quark mass $m_b(M_Z)$ in the $\overline{\rm MS}$ scheme with statistical (stat), experimental (exp) and hadronization (had) uncertainties. In the last column the measured pole mass M_b is listed.

O	$m_b(M_Z)\,[\mathrm{GeV}/c^2]$	$\pm$(stat)	$\pm$(exp)	$\pm$(had)	$M_b\,[\mathrm{GeV}/c^2]$
R_3	2.76	0.28	0.28	0.62	3.65
y_{3_1}	3.34	0.22	0.22	0.38	4.73

100% correlated. A similar difference of measured masses was reported in Ref. [8], where different clustering algorithms for the three-jet rate were studied. The results obtained for the pole mass by fitting the predictions in the pole mass scheme are also given in Table 5.

As is observed from Table 5, the first moment of the y_3 distribution allows for a mass measurement with better statistical and experimental accuracy than the three-jet rate. Furthermore, the hadronization uncertainty is considerably smaller. Therefore the result from this observable is quoted as the final b-quark mass value. The theoretical uncertainty is estimated as described in Section 5.1 by evaluating the impact of the uncertainty on the strong coupling constant and the renormalization scale variation. Because the pole and the running mass scheme are equivalent at NLO, the average of the values found for the two schemes is quoted as the final result, and half of the difference is taken as an additional theoretical systematic uncertainty due to the scheme ambiguity. This leads to a measurement of the b-quark mass of

$$m_b(M_Z) = [3.27 \pm 0.22(\mathrm{stat}) \pm 0.22(\mathrm{exp}) \pm 0.38(\mathrm{had}) \pm 0.16(\mathrm{theo})]\ \mathrm{GeV}/c^2 \quad .$$

The result obtained is in agreement with the measurements of DELPHI [5] and Brandenburg et al. [8]. The world average value from low-energy measurements is $m_b(m_b) = 4.2 \pm 0.1\,\mathrm{GeV}/c^2$ [32]. Using a two-loop running equation for the quark mass, this average value can be translated to $m_b(M_Z) = 2.89 \pm 0.08\,\mathrm{GeV}/c^2$, which is also in agreement with the result obtained here. This comparison is illustrated in Fig. 5, together with the other results. The result for the pole mass is

$$M_b = [4.73 \pm 0.29(\mathrm{stat}) \pm 0.29(\mathrm{exp}) \pm 0.49(\mathrm{had}) \pm 0.18(\mathrm{theo})]\,\mathrm{GeV}/c^2.$$

In this case the theoretical uncertainty is estimated from the renormalization scale variation only.

6 Test of the flavour independence of α_s

All the previous considerations are based on the assumption of flavour independence of the strong coupling constant, which in particular means that the strong coupling is the same for b quarks as for light quarks ($l = uds$), i.e., $\alpha_s^b = \alpha_s^l$. However, the measurement of R_{bd}^{pert} can also be used as a test of the flavour independence, if the b-quark mass is known. The ratio of the strong coupling constant for b and light quark events can be written up to NLO as

$$\frac{\alpha_s^b}{\alpha_s^l} = \left[R_{bd}^{\mathrm{pert}} - K(r_b(M_Z))\right] + a_1 \frac{\alpha_s(M_Z)}{\pi}\left[R_{bd}^{\mathrm{pert}} - K(r_b(M_Z)) - 1\right] \quad , \tag{13}$$

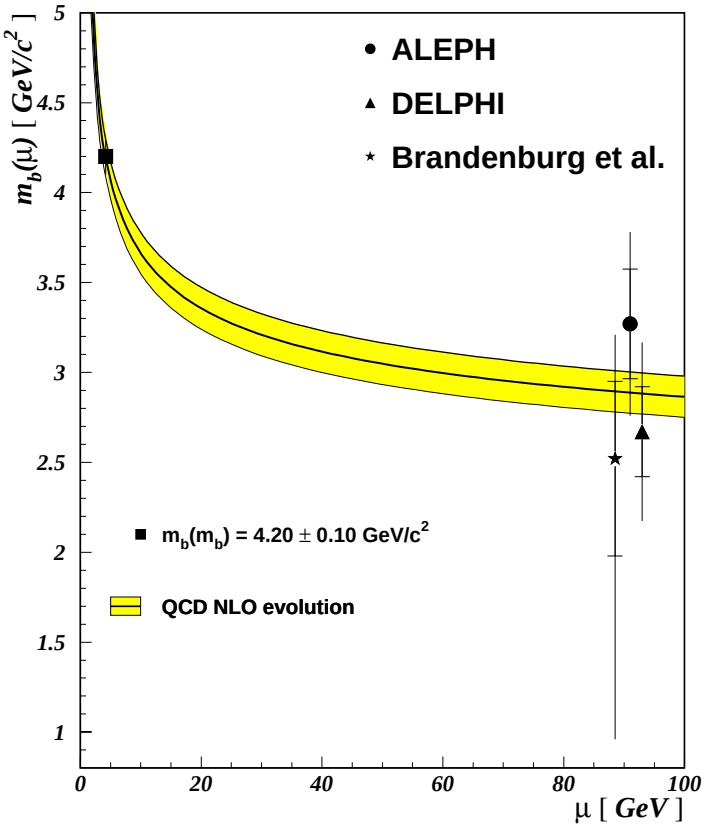

Figure 5: Comparison of the ALEPH result for $m_b(M_Z)$ with the world average value of low-energy measurements for $m_b(m_b)$, which is evolved up to the M_Z scale using a two-loop evolution equation with $\alpha_s(M_Z) = 0.119 \pm 0.003$. Also shown are the measurements by DELPHI [5] and Brandenburg et al. [8]. The inner error bars indicate the quadratic sum of the statistical and experimental uncertainties. The three points at the Z pole are separated for clarity.

where $K(r_b(M_Z))$ is the mass correction in Eqn. 6 and $a_1 = 6.073$ when using the first moment of the y_3 distribution as observable. Equation 13 is derived assuming $\alpha_s^b = \alpha_s^l(1+\delta)$, $\delta \ll 1$, and neglecting all terms of order $(\alpha_s^l)^2$ and $\alpha_s^l\,\delta$, so $\alpha_s(M_Z) = 0.119 \pm 0.003$ can be used for the coefficient of the next-to-leading order term. The coefficient a_1 was computed with EVENT. Taking an average b-quark mass of $m_b(m_b) = 4.2 \pm 0.1\,\mathrm{GeV}/c^2$ [32], and taking into account the scale uncertainties and scheme ambiguities as described in Section 5.1, the term $K(r_b(M_Z))$ amounts to -0.041 ± 0.003. Inserting the measured value R_{bd}^{pert} for the observable y_{3_1} results in

$$\frac{\alpha_s^b}{\alpha_s^l} = 0.997 \;\pm\; 0.004\,(\mathrm{stat}) \;\pm\; 0.004\,(\mathrm{exp}) \;\pm\; 0.007\,(\mathrm{had}) \;\pm\; 0.003\,(\mathrm{theo}) \quad ,$$

which is a confirmation of the flavour independence at a precision level of 1%. This constitutes an improvement in precision by a factor of two compared to a previous ALEPH analysis [33]. Recently, similar results were obtained by other experiments [5, 6, 7].

7 Conclusions

The effect of the b-quark mass has been studied on the ratios of observables in b and light quark decays of the Z boson in e^+e^- annihilation. Taking the first moment of the y_3 distribution, which has the smallest hadronization corrections and systematic uncertainties, a b-quark mass of

$$m_b(M_Z) = [3.27 \pm 0.22(\text{stat}) \pm 0.22(\text{exp}) \pm 0.38(\text{had}) \pm 0.16(\text{theo})] \text{ GeV}/c^2$$

is found, which is in agreement with recent measurements by other experiments [5, 8] and with measurements at lower energies. The three-jet rate defined by the `DURHAM` algorithm with $y_{\text{cut}} = 0.02$ turns out to be more sensitive to the details of the hadronization modelling.

The determination of the ratio of the first moment of the y_3 distribution in b and light quark events has alternatively been employed, along with previous measurements of the b-quark mass, to test the flavour independence of the strong coupling constant with a precision of 1.0%.

8 Acknowledgements

We would like to thank G. Rodrigo and P. Nason for providing us with theoretical input. Furthermore we would like to thank J. Fuster and S. Marti i Garcia for many interesting discussions on the subject.

We wish to thank our colleagues from the accelerator divisions for the successful operation of LEP. It is also a pleasure to thank the technical personnel of the collaborating institutions for their support in constructing and maintaining the ALEPH experiment. Those of the collaboration not from member states thank CERN for its hospitality.

References

[1] G. Rodrigo, QCD96 Montpellier, hep-ph/9609213 and Nucl. Phys. Proc. Suppl. **54A** (1997) 60.

[2] G. Rodrigo, M. Bilenky, and A. Santamaria, Phys. Rev. Lett. **79** (1997) 193.

[3] W. Bernreuther, A. Brandenburg, and P. Uwer, Phys. Rev. Lett. **79** (1997) 189.

[4] P. Nason and C. Oleari, Phys. Lett. **B407** (1997) 57.

[5] DELPHI Collaboration, *m_b at M_Z*, Phys. Lett. **B418** (1998) 430.

[6] OPAL Collaboration, *Test of the Flavour Independence of α_s Using Next-to-leading Order Calculations for Heavy Quarks*, Eur. Phys. J. **C11** (1999) 643.

[7] SLD Collaboration, *An Improved Test of the Flavour Independence of Strong Interactions*, Phys. Rev. **D59** (1999) 12002.

[8] A. Brandenburg et al., Phys. Lett. **B468** (1999) 168.

[9] C. Caso et al., Particle Data Group, Eur. Phys. J. **C3** (1998) 1.

[10] K. Hagiwara, T. Kuruma, and Y. Yamada, Nucl. Phys. **B358** (1991) 80;
G. Rodrigo, private communication.

[11] S. Catani et al., Phys. Lett. **B269** (1991) 179;
N. Brown and J. Stirling, Z. Phys. **C53** (1992) 629.

[12] ALEPH Collaboration, *Studies of Quantum Chromodynamics with the ALEPH Detector*, Phys. Rep. **294** (1998) 1.

[13] S. Catani, G. Turnock, and B.R. Webber, Phys. Lett. **B295** (1992) 269.

[14] ALEPH Collaboration, *ALEPH: A Detector for Electron-Positron Annihilations at LEP*, Nucl. Instr. Meth. **A294** (1990) 121.

[15] B. Mours et al., Nucl. Instr. Meth. **A379** (1996) 101.

[16] ALEPH Collaboration, *Performance of the ALEPH Detector at LEP*, Nucl. Instr. Meth. **A360** (1995) 481.

[17] T. Sjöstrand, Comp. Phys. Comm. **82** (1994) 74.

[18] C. Peterson et al., Phys. Rev. **D27** (1983) 105.

[19] R. Brun et al., CERN DD/EE/84-1 (1987).

[20] The LEP Collaborations ALEPH, DELPHI, L3, OPAL, the LEP Electroweak Working Group and the SLD Heavy Flavour and Electroweak Groups, *A combination of preliminary electroweak measurements and constraints on the Standard Model*, CERN-EP-2000-016, January 2000.

[21] ALEPH Collaboration, *A precise measurement of* $\Gamma_Z \to b\bar{b}/\Gamma_Z \to hadrons$, Phys. Lett. **B313** (1993) 535.

[22] ALEPH Collaboration, *Heavy flavour production and decay with prompt leptons in the ALEPH detector*, Z. Phys. **C62** (1994) 179.

[23] Z. Trocsanyi, JHEP **0001** (2000) 014.

[24] G. Marchesini et al., Comp. Phys. Comm. **67** (1992) 465.

[25] ALEPH Collaboration, *Measurement of the effective b quark fragmentation function at the Z peak*, ALEPH 2000-020, CONF 2000-017, contribution to the 2000 winter conferences.

[26] SLD Collaboration, *Precise measurement of the b-quark fragmentation function in* Z^0 *boson decays*, Phys. Rev. Lett. **8**4 (2000) 4300.

[27] M.G. Bowler, Z. Phys. **C11** (1981) 169.

[28] P. Nason, private communication, 1998.

[29] Z. Kunszt and P. Nason, private communication;
G. Altarelli, R. Kleiss, and C. Verzegnassi, *Z Physics at LEP1*, CERN Yellow Report 89-08, vol. 1, p. 373.

[30] R.K. Ellis, D.A. Ross, A.E. Terrano, Nucl. Phys. **B178** (1981) 421.

[31] S. Bethke, *Standard Model Physics*, hep-ex/0001023, January 2000.

[32] A. Pich, *Aspects of Quantum Chromodynamics*, hep-ph/000118, January 2000.

[33] ALEPH Collaboration, *Test of the Flavour Independence of* α_s, Phys. Lett. **B355** (1995) 381.